Interlayer exchange coupling between next nearest neighbor layers

Jae-Ho Han and Hyun-Woo Lee
PCTP and Department of Physics, Pohang University of Science and Technology, Pohang 790-784, Korea
(Received 11 June 2012; published 27 November 2012)

Interlayer exchange coupling (IEC) between next nearest neighbor magnetic layers is investigated. For a multilayer system that contains three magnetic layers (with magnetization directions $\hat{\mathbf{m}}_1$, $\hat{\mathbf{m}}_2$, and $\hat{\mathbf{m}}_3$, respectively) separated by two nonmagnetic layers, the angle dependence of the coupling energy and the thickness dependence of coupling constants were obtained. In addition to the well known nearest neighbor IEC of the form $-\tilde{J}_{12}\hat{\mathbf{m}}_1 \cdot \hat{\mathbf{m}}_2$ and $-\tilde{J}_{23}\hat{\mathbf{m}}_2 \cdot \hat{\mathbf{m}}_3$, we find the next nearest neighbor IEC of the form $-\tilde{J}_{123}(\hat{\mathbf{m}}_1 \cdot \hat{\mathbf{m}}_2)(\hat{\mathbf{m}}_2 \cdot \hat{\mathbf{m}}_3)$, which is different from the Heisenberg type next nearest neighbor coupling $-J_{13}\hat{\mathbf{m}}_1 \cdot \hat{\mathbf{m}}_3$. The strength of the next nearest neighbor IEC oscillates with respect to the thickness of both magnetic and nonmagnetic layers. The strength of the next nearest neighbor IEC is generally smaller than the conventional nearest neighbor IEC, but is large enough to allow for experimental detection.

DOI: 10.1103/PhysRevB.86.174426 PACS number(s): 75.30.Et, 75.70.Cn

I. INTRODUCTION

Since the discovery of giant magnetoresistance (GMR) in the late 1980's,[1,2] magnetic multilayer systems have received much attention and have been studied extensively. One of the heavily examined properties is the coupling between magnetic layers, which is called interlayer exchange coupling (IEC). The leading order term of IEC between two adjacent magnetic layers has a form $E/A = -J\hat{\mathbf{m}}_1 \cdot \hat{\mathbf{m}}_2$, where E is the exchange coupling energy, A is the cross sectional area of the multilayers, $\hat{\mathbf{m}}_1$ and $\hat{\mathbf{m}}_2$ are unit vectors along the magnetization of the two magnetic layers, and J is the IEC constant. If $J > 0$, a parallel configuration is preferred (ferromagnetic coupling) and if $J < 0$, an antiparallel configuration is preferred (antiferromagnetic coupling).

When the two magnetic layers are separated by a nonmagnetic spacer layer located in between, the coupling constant J between the two magnetic layers has an oscillatory dependence on the thickness of the spacer layer. This oscillation was first observed in Fe/Cr, Co/Cr, and Co/Ru superlattice structures,[3] and systematically studied for various systems thereafter. For samples with ferromagnetic Co layers, various choices of nonmagnetic spacer layers such as V, Mo, Rh, Cu, and Re produce an oscillation with a period 1–2 nm (Refs. 4–8) when samples are grown by sputtering. For samples grown by molecular-beam epitaxy, an additional oscillation with a shorter period is observed in Co/Cu, Cr/Fe, Ag/Fe, and Au/Fe samples.[9–16]

This oscillatory behavior of J is due to the presence of a sharp Fermi surface and the formation of quasibound states in spacer layers.[17–20] Since electrons are reflected at the ferromagnetic/nonmagnetic layer interfaces, the quasibound states are formed in the spacer layers. When the thickness of the spacer increases, the energies of the quasibound states change and cross the Fermi level periodically. This crossing gives rise to the variation of J with respect to the spacer layer thickness. It was demonstrated[19] that critical spanning vectors in the Fermi surface of the spacer affect the variation most strongly and determine the periods of the variation.

In later studies on multilayer systems containing just two magnetic layers, such as NFNFN (F: ferromagnetic metal; N: nonmagnetic metal), it was found that the IEC constant J between the two magnetic layers is not completely fixed by the central N layer and its interfaces with the two neighboring F layers. The oscillation of J with respect to the thickness of the ferromagnetic layers was observed in Co/Cu systems.[21] Moreover, oscillation with respect to the thickness of the capping layer (uppermost N layer) was also observed.[22] Thus the IEC in the central trilayer FNF does depend on system configurations outside the central trilayer. This dependence may be counterintuitive but is consistent with the quantum well state picture: Since quasibound states are not strictly localized at the central N layer, their energy levels and J may depend on the outside configuration.[23]

Implications of the quantum well picture are not limited to the thickness dependence. In an FNFNF structure, for instance, the quantum well picture implies that J for the IEC between the first two magnetic layers may depend on the magnetization vector at the third magnetic layer, thereby generating the effective IEC between next nearest magnetic layers (between the first and third magnetic layers).

The IEC is an important factor affecting the energy landscape of magnetic multilayer structures and the knowledge of next nearest neighbor (NNN) IEC will be helpful to design the energy landscape more accurately. One particular example where the energy landscape is important is current-driven magnetization switching through the spin-transfer torque (STT) mechanism.[24–26] Such switching has a high application potential towards nonvolatile memory and logic devices.[27–30] Recalling that practical STT switching devices employ three or more magnetic layers to minimize unwanted long-range magnetostatic interactions,[31,32] NNN IEC becomes relevant and modifies the energy landscape of the devices, which in turn affects the energy cost for the switching operation and the thermal stability of stored information. Thus to achieve energy-friendly devices with a long information retention time, the energy landscape of the devices needs to be carefully designed, to which the knowledge of NNN IEC can contribute.

Another important direction of research for the current-driven magnetization switching is to enhance the magnitude of the spin-transfer torque, which is desired for faster device operation. Interestingly, IEC is directly connected to the so-called perpendicular spin-transfer torque.[33,34] Recently there

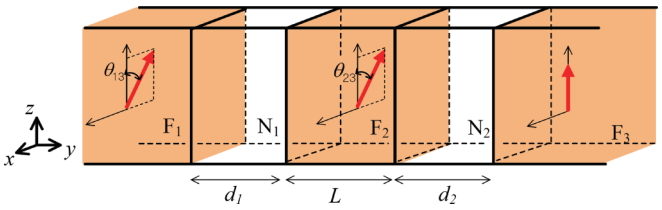

FIG. 1. (Color online) Schematic figure of the FNFNF structure. Two ferromagnetic layers, F_1 and F_3, are semi-infinite, and the other layers have a finite thickness with lengths given in the figure. Magnetizations are all in the same plane (x-z plane).

were efforts[35–42] to understand the properties of the perpendicular spin-transfer torque, and the existence of NNN IEC implies that NNN effects may exist even for the perpendicular spin-transfer torque, which may be useful for more accurate assessment of the perpendicular spin-transfer torque.

In this paper, we explore this NNN IEC by using a simple free-electron model. We found that the NNN IEC is generally weaker than the conventional nearest neighbor (NN) IEC but may be comparable in certain situations. We also found that both types of IEC have oscillatory dependence on the thickness of layers, but specific forms of the dependence are different for the two types of IEC.

II. FREE-ELECTRON MODEL

A. System and calculation scheme

Figure 1 shows schematically the FNFNF system that we are considering. In this configuration, interactions between F_1 and F_2, and between F_2 and F_3 are an ordinary NN IEC, whereas the interaction between F_1 and F_3 is a NNN IEC, which is the theme of this paper. All magnetizations of the ferromagnetic layers are assumed to be in the layer plane (x-z plane) and the magnetization of F_3 is fixed to the z axis without loss of generality since we expect that the total IEC energy does not change when all magnetization directions are simultaneously rotated by the same angle. In F_1 and F_2, the angle between the magnetization and z axis is θ_{i3} ($i = 1,2$). For simplicity, we assume that the saturation magnetizations are the same for all ferromagnetic layers, conduction electrons interact with the magnetizations through an s–d type interaction, and no impurities are present.

In theoretical works, IEC was investigated[17–20] usually by evaluating the total energy of systems as a function of magnetization directions. In view of its relevance to emerging applications of magnetic multilayer systems based on the spin-transfer torque, here we evaluate it by calculating instead the torque exerted on the magnetization. Although this torque approach is less direct than the total energy approach, it is illustrative in clarifying the connection between IEC and the spin-transfer torque. When the angle of a magnetization is changed, the energy of IEC changes and a torque arises. For instance, the conventional NN IEC $-J\hat{\mathbf{m}}_2 \cdot \hat{\mathbf{m}}_3$ generates a torque proportional to $-J\hat{\mathbf{m}}_2 \times \hat{\mathbf{m}}_3$ (magnitude $-J \sin\theta_{23}$) on $\hat{\mathbf{m}}_3$. In the sense that IEC is an interaction mediated by the conduction electrons (here, we assume the carrier of charge and spin to be electrons), it has the same origin as the spin-transfer torque. Actually the perpendicular spin-transfer torque acting on F_3 is also proportional to $\hat{\mathbf{m}}_2 \times \hat{\mathbf{m}}_3$, and it is known that at zero voltage bias the perpendicular spin-transfer torque is identical to the torque due to the IEC. Therefore, we calculate torque as a function of magnetization angles, and integrate it with respect to the angle of the magnetization to evaluate the total IEC energy. By the way, we will ignore the so-called in-plane spin-transfer torque proportional to $\hat{\mathbf{m}}_3 \times (\hat{\mathbf{m}}_2 \times \hat{\mathbf{m}}_3)$ since it vanishes at zero voltage bias[24,33] and is irrelevant for IEC.

The calculation scheme is as follows. First, one solves the one-electron Schrödinger equation. In nonmagnetic layers, a conduction electron is subject to a spin-independent potential energy. In magnetic layers, however, the conduction electron and magnetization interact via the s-d exchange interaction, which gives rise to a spin-dependent potential energy for a conduction electron proportional to $\boldsymbol{\sigma} \cdot \hat{\mathbf{m}}$, where $\boldsymbol{\sigma}$ is the Pauli matrix representing the conduction electron spin and $\hat{\mathbf{m}}$ is the unit vector along the magnetization direction of the magnetic layer. Then the spin currents are calculated from the wave function, and one adds up this spin current for all occupied conduction electrons. This total spin current has a spatial dependence. Then the torque acting on a ferromagnetic layer can be evaluated from the difference between the incoming spin current at the left interface of the magnetic layer and the outgoing spin current at the right interface of the magnetic layer.[34] Finally, the IEC energy can be obtained by integrating the torque over the magnetization angle. By the way, our explicit calculation results confirm that the torque is indeed along the direction $\hat{\mathbf{m}}_3 \times \hat{\mathbf{m}}_2$ and the in-plane torque $\hat{\mathbf{m}}_3 \times (\hat{\mathbf{m}}_3 \times \hat{\mathbf{m}}_2)$ is absent, justifying our approach to evaluate IEC from the perpendicular spin-transfer torque at zero bias.

B. One-electron Schrödinger equation

The dynamics of an electron in the multilayer can be described by the following one-electron Schrödinger equation,

$$-\frac{\hbar^2}{2m}\nabla^2\Psi_s(x,y,z) + U_{ss'}(y)\Psi_{s'}(x,y,z) = E\Psi_s(x,y,z), \quad (1)$$

where

$$U_{ss'}(y) = \begin{cases} -\Delta(\boldsymbol{\sigma}\cdot\hat{\mathbf{m}})_{ss'} & \text{(in F's)}, \\ E_c\delta_{ss'} & \text{(in N's)}. \end{cases} \quad (2)$$

$\boldsymbol{\sigma} = (\sigma^x,\sigma^y,\sigma^z)$, $\sigma^{x,y,z}$ is the Pauli matrix, and $\hat{\mathbf{m}}$ is $\hat{\mathbf{m}}_1$, $\hat{\mathbf{m}}_2$, and $\hat{\mathbf{m}}_3$ when an electron is in F_1, F_2, and F_3, respectively. Δ is the exchange interaction constant, E_c is the conduction band bottom energy, and m is the effective mass of an electron. s and s' ($=\pm$) are indices of spin space with the z axis chosen as the spin quantization axis, and $\delta_{ss'}$ is the Kronecker delta. The summation over the repeated index s' is implicit in Eq. (1).

Since there is translational symmetry in the layer plane direction (x, z direction), we can factorize $\Psi_s(x,y,z)$ as $\Psi_s(x,y,z) = \frac{1}{\sqrt{V}}e^{ik_x x}e^{ik_z z}\psi_s(y) = \frac{1}{\sqrt{V}}e^{i\vec{k}_\parallel\cdot\vec{r}_\parallel}\psi_s(y)$, where $\vec{k}_\parallel$, $\vec{r}_\parallel$ are the in-plane component of the wave vector and position vector, and V is the total volume of the system which tends to infinity. Substituting this into Eq. (1) yields the equation for $\psi_s(y)$,

$$-\frac{\hbar^2}{2m}\frac{d^2}{dy^2}\psi_s(y) + U_{ss'}(y)\psi_{s'}(y) = \epsilon\psi_s(y), \quad (3)$$

where $\epsilon = E - \hbar^2 k_\parallel^2/2m$.

Within each ferromagnetic layer, U is diagonalized by choosing a quantization axis parallel to the magnetization. In this axis choice, $U = \mathrm{diag}(U_\uparrow, U_\downarrow)$, where $\uparrow$ and $\downarrow$ denote the majority and minority spin component, respectively, and $U_{\uparrow,\downarrow} = \mp\Delta$. Because the potential $U(y)$ is spatially uniform within each layer, the solution of Eq. (3) in each layer is a linear combination of plane waves. Explicitly,

$$\begin{aligned}\psi^{F_a}_{\uparrow,\downarrow} &= A^a_{\uparrow,\downarrow} e^{ik_{\uparrow,\downarrow} y} + B^a_{\uparrow,\downarrow} e^{-ik_{\uparrow,\downarrow} y},\\ \psi^{N_b}_{\pm} &= C^b_{\pm} e^{i\kappa y} + D^b_{\pm} e^{-i\kappa y},\end{aligned} \tag{4}$$

where $k_{\uparrow,\downarrow} = \sqrt{\epsilon - U_{\uparrow,\downarrow}}/\hbar$, $\kappa = \sqrt{\epsilon - E_c}/\hbar$, a (=1,2,3) indicates each ferromagnetic layer, and b (=1,2) indicates each nonmagnetic layer. In a FNFNF system, there are thus 5 (layers) $\times$ 2 (spin components) $\times$ 2(longitudinal momentum directions)=20 coefficients, which should satisfy the boundary conditions arising from the wave function matching at the interfaces between layers. Since the spin quantization axes in magnetic layers are in general different from the z axis, which we choose as the spin quantization axis in nonmagnetic layers, the wave function matching at each interface between a magnetic and nonmagnetic layer generates the following four boundary conditions: two for the continuity of wave functions,

$$\begin{aligned}\psi^N_+ &= \psi^F_\uparrow \cos(\theta/2) + \psi^F_\downarrow \sin(\theta/2),\\ \psi^N_- &= -\psi^F_\uparrow \sin(\theta/2) + \psi^F_\downarrow \cos(\theta/2),\end{aligned}$$

and the other two for the continuity of the derivatives of wave functions,

$$\begin{aligned}\frac{d\psi^N_+}{dy} &= \frac{d\psi^F_\uparrow}{dy}\cos(\theta/2) + \frac{d\psi^F_\downarrow}{dy}\sin(\theta/2),\\ \frac{d\psi^N_-}{dy} &= -\frac{d\psi^F_\uparrow}{y}\sin(\theta/2) + \frac{d\psi^F_\downarrow}{dy}\cos(\theta/2),\end{aligned}$$

where θ is the angle between the two different spin quantization axes in the two neighboring layers. Since there are four interfaces in a FNFNF system, four (=$20 - 4 \times 4$) independent coefficients remain to be determined. These four coefficients are determined by choosing four scattering states: (i) electrons with a majority spin component injected from the left ($A^{F_1}_\uparrow = 1, A^{F_1}_\downarrow = B^{F_3}_\uparrow = B^{F_3}_\downarrow = 0$), (ii) electrons with a minority spin component injected from the left ($A^{F_1}_\downarrow = 1, A^{F_1}_\uparrow = B^{F_3}_\uparrow = B^{F_3}_\downarrow = 0$), (iii) electrons with a majority spin component injected from the right ($B^{F_3}_\uparrow = 1, A^{F_1}_\uparrow = A^{F_1}_\downarrow = B^{F_3}_\downarrow = 0$), and (iv) electrons with a minority spin component injected from the right ($B^{F_3}_\downarrow = 1, A^{F_1}_\uparrow = A^{F_1}_\downarrow = B^{F_3}_\uparrow = 0$). Thus these four scattering states exhaust the degrees of freedom and constitute a complete set of bases.

C. Spin current density and perpendicular spin torque

From the wave function $\Psi_s(x,y,z)$, we can calculate the spin current density j^{spin}_i for each scattering state. Here, i denotes the spin direction (x, y, or z) and the direction of motion is chosen to be y since only this direction of motion is relevant in the present situation. Then the spin current density generated by an electron in the state Ψ_s is given by

$$\begin{aligned}j^{\mathrm{spin}}_i &= \frac{1}{m}\mathrm{Re}\left[\Psi^\dagger_s \left(\frac{\hbar}{i}\frac{\partial}{\partial y}\right)\left(\frac{\hbar}{2}\sigma^i_{ss'}\right)\Psi_{s'}\right]\\ &= \frac{1}{mV}\mathrm{Re}\left[\psi^\dagger_s(y)\left(\frac{\hbar}{i}\frac{d}{dy}\right)\left(\frac{\hbar}{2}\sigma^i_{ss'}\right)\psi_{s'}(y)\right],\end{aligned} \tag{5}$$

where $\mathrm{Re}(\omega)$ is the real part of complex number ω.

j^{spin}_i in the above is the spin current density for one electron, and we have to sum it up to Fermi energy to get the total spin current density. First, let us consider the scattering state in which spin-up electrons are injected from the left [case (i)]. Since electrons are filled up to a Fermi energy of F_1, and only electrons with $k_y > 0$ ($\epsilon = \hbar^2 k_y^2/2m$) can be injected, we have a total spin current density $J^{\mathrm{spin}}_i(L, \uparrow)$ due to these spin-up electrons injected from the left as

$$\begin{aligned}J^{\mathrm{spin}}_i(L,\uparrow) &= \sum_{k<k^\uparrow_{F_1}, k_y>0} j^{\mathrm{spin}}_i(\epsilon(k_y))\\ &= \frac{V}{2}\int_{k<k^\uparrow_{F_1}} \frac{d^3k}{(2\pi)^3} j^{\mathrm{spin}}_i(\epsilon(k_y))\\ &= \frac{\hbar^2}{4m}\int_{k<k^\uparrow_{F_1}} \frac{d^3k}{(2\pi)^3}\mathrm{Im}\left[\psi^\dagger_s \sigma^i_{ss'}\frac{d}{dy}\psi_{s'}\right],\end{aligned} \tag{6}$$

where $k^\uparrow_{F_1}$ is the Fermi wave vector of majority electrons in F_1 and $\mathrm{Im}(\omega)$ is the imaginary part of the complex number ω. Similarly, the spin current for the other scattering states (ii), (iii), and (iv) can be calculated as $J^{\mathrm{spin}}_i(L,\downarrow)$, $J^{\mathrm{spin}}_i(R,\uparrow)$, and $J^{\mathrm{spin}}_i(R,\downarrow)$, respectively. The total spin current density $J^{\mathrm{spin,total}}_i$ is

$$\begin{aligned}J^{\mathrm{spin,total}}_i &= J^{\mathrm{spin}}_i(L,\uparrow) + J^{\mathrm{spin}}_i(L,\downarrow)\\ &\quad + J^{\mathrm{spin}}_i(R,\uparrow) + J^{\mathrm{spin}}_i(R,\downarrow).\end{aligned} \tag{7}$$

Since $\hat{\mathbf{m}}_3 \times \hat{\mathbf{m}}_2$ is along the y direction, the perpendicular spin torque (perpendicular to the plane spanned by magnetizations) exerted on F_3 can be calculated by using a total spin current density due to the angular momentum conservation. The perpendicular component of the angular momentum absorbed by F_3 per unit time per unit area is $J^{\mathrm{spin,total}}_y$ within N_3 ($J^{\mathrm{spin,total}}_y$ is conserved in N_3), which is minus the perpendicular spin-transfer torque per unit area (from the angular momentum conservation):

$$\tau_3/A = -J^{\mathrm{spin,total}}_y. \tag{8}$$

III. RESULTS

Figure 2 shows perpendicular torque τ_3 in terms of the angle θ_{23} between $\hat{\mathbf{m}}_2$ and $\hat{\mathbf{m}}_3$, while the angle $\theta_{13} - \theta_{23}$ between $\hat{\mathbf{m}}_1$ and $\hat{\mathbf{m}}_2$ is fixed. The parameters used in calculations are as follows: $\Delta = 1.96$ eV, $E_c = -1$ eV, $E_F = 2.62$ eV, $d_1 = d_2 = 1$ nm, $L = 2$ nm.[24,33,43] The black solid curve in Fig. 2 is the result for $\theta_{13} = \theta_{23}$ ($\hat{\mathbf{m}}_1 = \hat{\mathbf{m}}_2$), while the blue dashed curve is for $\theta_{13} = \theta_{23} + \pi$ ($\hat{\mathbf{m}}_1 = -\hat{\mathbf{m}}_2$). In both cases, τ_3 shows the sine behavior as a function of θ_{23}, $\tau_3/A = -J_{23}\sin\theta_{23}$, implying that the total IEC energy is proportional to $\cos\theta_{23} = \hat{\mathbf{m}}_2 \cdot \hat{\mathbf{m}}_3$ when the difference $\theta_{13} - \theta_{23}$ (or $\hat{\mathbf{m}}_1 \cdot \hat{\mathbf{m}}_2$) is fixed. In the two cases, however, the amplitudes J_{23} of the sine

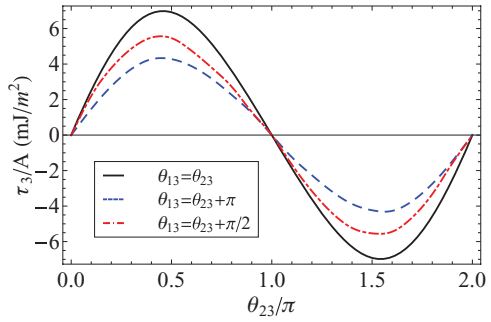

FIG. 2. (Color online) τ_3 vs θ_{23} for parallel ($\hat{\mathbf{m}}_1 = \hat{\mathbf{m}}_2, \theta_{13} = \theta_{23}$), antiparallel ($\hat{\mathbf{m}}_1 = -\hat{\mathbf{m}}_2$, $\theta_{13} = \theta_{23} + \pi$), and perpendicular ($\hat{\mathbf{m}}_1 \perp \hat{\mathbf{m}}_2$, $\theta_{13} = \theta_{23} + \pi/2$) configurations. All have the same sinusoidal form but with different amplitudes.

oscillation are different, implying that J_{23} does depend on $\hat{\mathbf{m}}_1 \cdot \hat{\mathbf{m}}_2$. We find $J_{23} = 5.59 \pm 1.32$ mJ/m^2 for $\hat{\mathbf{m}} = \pm\hat{\mathbf{m}}_2$. Here 1.32 mJ/m^2 is a measure of how sensitively the IEC between F_2 and F_3 depends on the configuration in F_1. Note that this is smaller than but not negligible compared to the average value of 5.59 mJ/m^2. To investigate the dependence of J_{23} on $\hat{\mathbf{m}}_1 \cdot \hat{\mathbf{m}}_2$, we calculate τ_3 as a function of θ_{23} when $\hat{\mathbf{m}}_1 \cdot \hat{\mathbf{m}}_2$ is fixed to 0 (red dashed-dotted curve in Fig. 2). Again τ_3/A is excellently fitted by the sine curve $-J_{23} \sin\theta_{23}$ if we choose $J_{23} = 5.46$ mJ/m^2. Note that this value agrees with the average value of 5.59 mJ/m^2 of the two earlier cases, within 2% accuracy. Thus within this accuracy, the dependence of J_{23} on $\hat{\mathbf{m}}_1 \cdot \hat{\mathbf{m}}_2$ is described by $J_{23} = \tilde{J}_{23} + \tilde{J}_{123}\hat{\mathbf{m}}_1 \cdot \hat{\mathbf{m}}_2$ and we can write the torque as

$$\tau_3/A = -(\tilde{J}_{23} + \tilde{J}_{123}\hat{\mathbf{m}}_1 \cdot \hat{\mathbf{m}}_2)\sin\theta_{23}, \tag{9}$$

where $\tilde{J}_{23} = 5.59$ mJ/m^2 and $\tilde{J}_{123} = 1.32$ mJ/m^2 are constants independent of the relative directions of the magnetization vectors.

The IEC energy related to magnetic layer F_3 can be obtained by integrating the torque in Eq. (9) with respect to the angle $-\theta_{23}$, which yields $E/A = -\tilde{J}_{23}\hat{\mathbf{m}}_2 \cdot \hat{\mathbf{m}}_3 - \tilde{J}_{123}(\hat{\mathbf{m}}_1 \cdot \hat{\mathbf{m}}_2)(\hat{\mathbf{m}}_2 \cdot \hat{\mathbf{m}}_3) + C_{12}$. The integration constant C_{12} is a function of the angle between magnetizations $\hat{\mathbf{m}}_1$ and $\hat{\mathbf{m}}_2$. One can perform a similar analysis for the torque τ_1 acting on $\hat{\mathbf{m}}_1$, as a function of the relative angle between $\hat{\mathbf{m}}_1$ and $\hat{\mathbf{m}}_2$, while the relative angle between $\hat{\mathbf{m}}_2$ and $\hat{\mathbf{m}}_3$ stays fixed. Through this analysis, we find $E/A = -\tilde{J}_{12}\hat{\mathbf{m}}_1 \cdot \hat{\mathbf{m}}_2 - \tilde{J}_{123}(\hat{\mathbf{m}}_1 \cdot \hat{\mathbf{m}}_2)(\hat{\mathbf{m}}_2 \cdot \hat{\mathbf{m}}_3) + C_{23}$, where the integration constant C_{23} is a function of the angle between $\hat{\mathbf{m}}_2$ and $\hat{\mathbf{m}}_3$. From these two analyses, we conclude that the total IEC energy is

$$E/A = -\tilde{J}_{12}\hat{\mathbf{m}}_1 \cdot \hat{\mathbf{m}}_2 - \tilde{J}_{23}\hat{\mathbf{m}}_2 \cdot \hat{\mathbf{m}}_3 - \tilde{J}_{123}(\hat{\mathbf{m}}_1 \cdot \hat{\mathbf{m}}_2)(\hat{\mathbf{m}}_2 \cdot \hat{\mathbf{m}}_3). \tag{10}$$

The first two terms on the right-hand side are conventional NN IEC's in the sense that they do not depend on the "outside" configuration ($\hat{\mathbf{m}}_3$ in the case of the first term and $\hat{\mathbf{m}}_1$ in the case of the second term). In the third term, in contrast, the NNN magnetizations $\hat{\mathbf{m}}_1$ and $\hat{\mathbf{m}}_3$ couple to each other through the inner products with the magnetization $\hat{\mathbf{m}}_2$ of the intervening layer. Although the third term is different from a pure NNN coupling ($\hat{\mathbf{m}}_1 \cdot \hat{\mathbf{m}}_3$), it still involves the NNN pair layers and we call it NNN IEC. Note that its strength constant $\tilde{J}_{123} =$ 1.32 mJ/m^2 is not negligible compared to the conventional NN IEC constant $\tilde{J}_{12} = \tilde{J}_{23} = 5.59$ mJ/m^2.

It is well known that the IEC is mediated by conduction electrons. Thus, to generate the NNN IEC in Eq. (10), the spin information should be carried by these electrons from one ferromagnetic layer (F_1) to the NNN layer (F_3) without being completely destroyed (or randomized) by the intermediate ferromagnetic layer (F_2). In this regard, the form of the NNN IEC can be understood as follows. When conduction electrons are incident onto a metallic ferromagnetic layer, the spin component of the conduction electrons perpendicular to the magnetization of the ferromagnetic layer decays rapidly[34] within a few atomic monolayers of the ferromagnetic layer. There are various mechanisms[34] contributing to the decay such as spin dephasing in the ferromagnet, spin-dependent reflection, and spin rotation at the ferromagnet-nonmagnet interface. Thus when $\hat{\mathbf{m}}_1 \cdot \hat{\mathbf{m}}_2 = 0$, the intermediate ferromagnetic layer (F_2) blocks almost completely the spin information propagation from F_1 to F_3. On the other hand, the longitudinal spin component of the conduction electrons parallel or antiparallel to the magnetization direction is not diminished by such mechanisms and can be maintained over a longer distance. Thus, if $\hat{\mathbf{m}}_1 \cdot \hat{\mathbf{m}}_2 \neq 0$, conduction electrons coming from F_1 can deliver its spin component parallel to the magnetization of F_2 ($\hat{\mathbf{m}}_2$), which is $(\hat{\mathbf{m}}_1 \cdot \hat{\mathbf{m}}_2)\hat{\mathbf{m}}_2$ to F_3, and give rise to the IEC proportional to $(\hat{\mathbf{m}}_1 \cdot \hat{\mathbf{m}}_2)(\hat{\mathbf{m}}_2 \cdot \hat{\mathbf{m}}_3)$ when they are incident on F_3. This IEC is nothing but the NNN IEC, the last term in Eq. (10). This mechanism also explains the absence of the pure Heisenberg-type NNN interaction $\tilde{J}_{13}\hat{\mathbf{m}}_1 \cdot \hat{\mathbf{m}}_3$; since the interaction between $\hat{\mathbf{m}}_1$ and $\hat{\mathbf{m}}_3$ is mediated by conduction electrons (we ignore the magnetic dipole interaction) and these electrons pass through F_2, the spin filtering effect in F_2 allows coupling of the form $\tilde{J}_{123}(\hat{\mathbf{m}}_1 \cdot \hat{\mathbf{m}}_2)(\hat{\mathbf{m}}_2 \cdot \hat{\mathbf{m}}_3)$ only for IEC. We find that this form of NNN IEC explains our calculation results excellently except those data obtained for a very small thickness L ($\lesssim$0.5 nm) of F_2 (Appendix B).

Next, we examine the thickness-dependent oscillation of NN and NNN IEC. The d_2 dependence of $\tilde{J}_{23}$ [Fig. 3(a)] has a single oscillation period of about 0.3 nm. This period arises from the critical spanning vector $2k_F$ (period $= 2\pi/2k_F$) of the spherical Fermi surface of N_2 (k_F is the Fermi wave vector in N_2).

$\tilde{J}_{23}$ depends on the thickness L of F_2 as well [Fig. 3(b)]. The L dependence is oscillatory, as discussed in Ref. 23, but unlike Ref. 23 we find that the L-dependent oscillation is a superposition of *two* oscillations with two different periods 0.3 and 0.75 nm, which agree with the periods corresponding to the critical spanning vectors $2k_{F_2}^{\uparrow}$ and $2k_{F_2}^{\downarrow}$ of the majority and minority Fermi surfaces of F_2, respectively. Here $k_{F_2}^{\uparrow}$ and $k_{F_2}^{\downarrow}$ are the Fermi wave vectors in F_2 for the majority and minority electrons. In contrast, the L dependence in Ref. 23 has only one oscillation period corresponding to the critical spanning vector of the minority Fermi surface of F_2 and the critical spanning vector of the majority Fermi surface does not lead to the oscillatory L dependence. We believe that this difference arises because Ref. 23 considered a special case where the majority electrons of F_2 do not get reflected at all at the interfaces between F_2 and N_2 and between F_2 and N_1. Our result in Fig. 3(b) indicates that when this special assumption

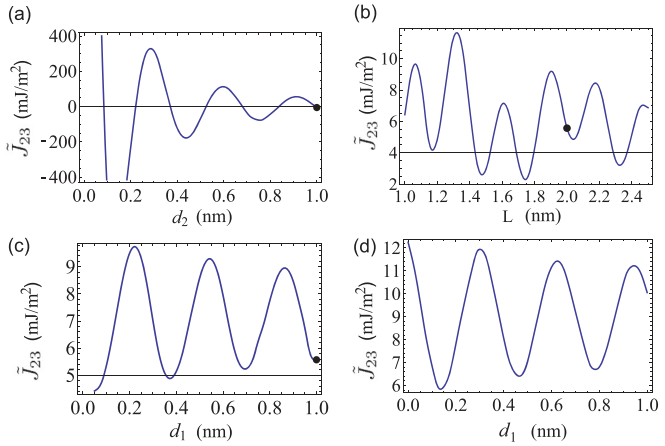

FIG. 3. (Color online) Thickness dependence of $\tilde{J}_{23}$ with respect to layer thicknesses. The reference thicknesses are $d_1 = d_2 = 1$ nm and $L = 2$ nm. (a) The d_1 dependence, (b) the L dependence, and (c) the d_1 dependence of the NN IEC constant $\tilde{J}_{23}$. In (a), (b), and (c), only one of the three thicknesses d_1, d_2, and L are varied while the other two remain at the reference values. (d) The d_1 dependence of $\tilde{J}_{23}$ at $L = 2.5$ nm with d_2 at the reference value. The black dots in (a), (b), and (c) are the points where Fig. 2 is calculated.

is lifted, the majority electrons also generate the oscillatory L dependence of $\tilde{J}_{23}$.

We find that $\tilde{J}_{23}$ depends on the thickness d_1 of N_1 as well [Figs. 3(c) and 3(d)]. The d_1 dependence exhibits oscillation with a single period corresponding to the critical spanning vector $2k_F$ of N_1. Note that the d_1-dependent oscillation may not be centered at zero [Figs. 3(c) and 3(d)]. This oscillation away from zero is understandable considering that the oscillation amplitudes of the d_2, L, and d_1 dependences of $\tilde{J}_{23}$ are getting progressively smaller. Thus when d_2 and L values prefer, say, large positive values of $\tilde{J}_{23}$, the d_1-dependent oscillation of $\tilde{J}_{23}$ is biased towards the positive side. We remark that the L dependence of $\tilde{J}_{23}$ is not centered at zero either.

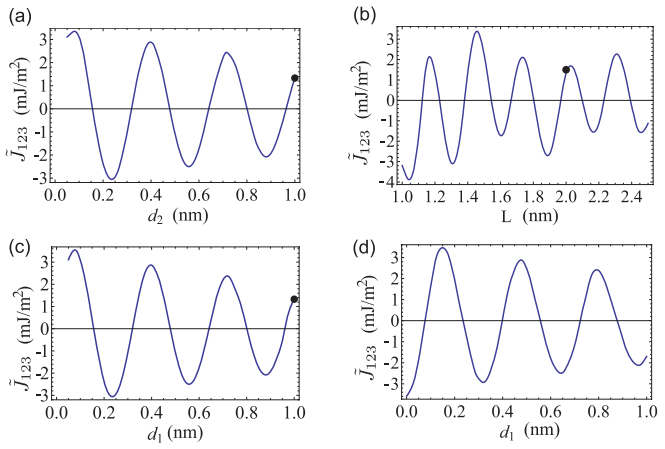

FIG. 4. (Color online) Thickness dependence of the NNN IEC constant $\tilde{J}_{123}$ with respect to layer thicknesses. (a) The d_1 dependence, (b) the L dependence, and (c) the d_1 dependence of the NNN IEC constant $\tilde{J}_{123}$. In (a), (b), and (c), only one of the three thicknesses d_1, d_2, and L are varied while the other two remain at the reference values. (d) The d_1 dependence of $\tilde{J}_{123}$ at $L = 2.5$ nm with d_2 at the reference value. The black dots in (a), (b), and (c) are the points where Fig. 2 is calculated.

The thickness dependences of the NNN IEC $\tilde{J}_{123}$ are shown in Fig. 4. Each of the d_1- and d_2-dependent oscillations [Figs. 4(c) and 4(a)] of $\tilde{J}_{123}$ has a single oscillation period (0.3 nm) determined by the critical spanning vector $2k_F$ of N_1 and N_2, and the L-dependent oscillation has two oscillation periods (0.3 and 0.75 nm) determined by the critical spanning vectors of $2k^{\uparrow}_{F_2}$ and $2k^{\downarrow}_{F_2}$, the majority and minority Fermi surfaces of F_2. Thus the oscillation periods of $\tilde{J}_{123}$ with respect to d_1, d_2, and L are identical to the corresponding periods of $\tilde{J}_{23}$. However, unlike the oscillations of $\tilde{J}_{23}$, the oscillations of $\tilde{J}_{123}$ are all centered at zero [Fig. 4(d)]. We attribute this difference to the fact that for the NNN IEC between F_1 and F_3, all three thicknesses d_1, L, and d_2 are length scales of the "spacer" between F_1 and F_3, whereas for the NN IEC between F_2 and F_3 and the thickness d_1 and L are length scales of the "outside" configurations.

IV. DISCUSSIONS

The numerical calculation results in Fig. 3 indicate that the NN IEC interaction strength oscillates not only when the spacer thickness changes but also when the thicknesses of the "outside" configuration change. The three types of oscillations (d_1, d_2, and L dependences) in Fig. 3 are qualitatively consistent with the following expression,

$$\tilde{J}_{23} = \mathrm{Im}\{e^{2ik_{N_2}d_2}[A + e^{2ik^{\uparrow}_{F_2}L}(B + Ce^{2ik_{N_1}d_1}) + e^{2ik^{\downarrow}_{F_2}L}(D + Ee^{2ik_{N_1}d_1})]\}, \quad (11)$$

which is a generalization of the theoretical results in Ref. 23. In Eq. (11), A, B, C, D, and E are nonoscillating decaying functions of d_1, d_2, and L. Equation (11) generalizes the result in Ref. 23 in two ways: (i) Spin-up electrons also experience scattering at the interfaces and are responsible for the term proportional to $\exp(2ik^{\uparrow}_{F_2}L)$. This term is absent in Ref. 23. (ii) The finite thickness d_1 of the "outside" normal metal layer gives rise to the oscillating factor $\exp(2ik_{N_1}d_1)$, which is again absent in Ref. 23 since $d_1 = \infty$ is assumed in Ref. 23. d_1-dependent oscillation was reported in the experiment.[22] When d_1, d_2, and L are sufficiently large, an analytic expression for $\tilde{J}_{23}$ can be derived (Appendix A) by generalizing the method in Ref. 23.

The numerical calculation results in Fig. 4 indicate the d_1-, d_2-, and L-dependent oscillations of the NNN IEC constant $\tilde{J}_{123}$. Since all these three oscillations of $\tilde{J}_{123}$ are centered at zero, the expression for $\tilde{J}_{123}$ should be different from Eq. (11). We expect that in the $F_1N_1F_2N_2F_3$ system the trilayer $N_1F_2N_2$ as a whole serves as a spacer for the IEC coupling between F_1 and F_3. Then, since the spacer itself contains a ferromagnetic layer, quasibound states in the spacer will be spin dependent, and spin-up and spin-down electrons will produce separately their own oscillations. Note that Figs. 4(a) and 4(c) are the same since N_1 and N_2 play a symmetric role in the spacer. Thus this expectation leads to the following expression,

$$\tilde{J}_{123} = \mathrm{Im}\big(\tilde{A}e^{2ik_{N_1}d_1+2ik^{\uparrow}_{F_2}L+2ik_{N_2}d_2} + \tilde{B}e^{2ik_{N_1}d_1+2ik^{\downarrow}_{F_2}L+2ik_{N_2}d_2}\big), \quad (12)$$

where $\tilde{A}$ and $\tilde{B}$ are nonoscillating decaying functions of d_1, d_2, and L. We remark that Eq. (12) is consistent with all qualitative features of the oscillations in Fig. 4. When d_1, d_2, and L are sufficiently large, an analytic expression for $\tilde{J}_{123}$ can be derived (Appendix A) by generalizing the method in Ref. 23.

Next we discuss the oscillation amplitude of the NNN IEC. In Fig. 4, the oscillation amplitude of the NNN IEC constant $\tilde{J}_{123}$ falls in the range 3–5 mJ/m^2. This value is much smaller than the spacer d_2-dependent oscillation amplitude of the NN IEC constant $\tilde{J}_{23}$ [Fig. 3(a)]. This explains why the NNN IEC has not been recognized in previous experiments. However, we remark that the oscillation amplitude of the NNN IEC is comparable to the amplitude of the "outside" layer thickness dependence of $\tilde{J}_{23}$ [Figs. 3(b)–3(d)]. Considering that the "outside" layer thickness dependence was measurable in the experiment,[22] we expect that the oscillation of the NNN IEC is also measurable in experiments. The experimental confirmation of the NNN IEC is most probable in situations when the NN IEC is suppressed. For the reference thicknesses $d_1 = d_2 = 1$ nm and $L = 2$ nm (black dots in Fig. 3), $\tilde{J}_{23}$ is only about 5 mJ/m^2. In this situation, if one varies only d_1 and L and keeps d_2 at the reference value, $\tilde{J}_{23}$ remains comparable to $\tilde{J}_{123}$, facilitating the experimental test of the NNN IEC.

We also remark that even though the results in Figs. 3 and 4 are obtained from a simple model that contains only one energy band, the main results such as the existence and the oscillation of the NNN IEC will persist even when a more realistic energy band structure is taken into account since the NNN IEC is governed by the critical spanning vectors of the Fermi surface, and this physics is not altered by complications in a realistic energy band structure.

Lastly, we explore the possibility of even longer-range coupling by examining the $F_1N_1F_2N_2F_3N_3F_4$ multilayer system. This system contains four magnetic layers and allows the examination of the next next nearest neighbor (NNNN) IEC. We again calculate the torque acting on the last ferromagnetic layer F_4 and integrate it over the angle θ_{34} (angles are defined in a similar way) to obtain the total IEC acting on F_4. To decompose the total IEC into NN, NNN, and NNNN components, we calculate the torque as a function of θ_{34} under three different configurations: (1) while maintaining $\hat{\mathbf{m}}_1//\hat{\mathbf{m}}_2//\hat{\mathbf{m}}_3$, (2) $\hat{\mathbf{m}}_1//-\hat{\mathbf{m}}_2//\hat{\mathbf{m}}_3$, and (3) $-\hat{\mathbf{m}}_1//-\hat{\mathbf{m}}_2//\hat{\mathbf{m}}_3$. The torque τ_4 has a sinusoidal dependence on θ_{34} in all three configurations. The oscillation amplitude difference between case (2) and (3) determines the strength of the NNNN IEC coupling $\tilde{J}_{1234}$ between F_1 and F_2 of the form $-\tilde{J}_{1234}(\hat{\mathbf{m}}_1 \cdot \hat{\mathbf{m}}_2)(\hat{\mathbf{m}}_2 \cdot \hat{\mathbf{m}}_3)(\hat{\mathbf{m}}_3 \cdot \hat{\mathbf{m}}_3)$. To evaluate $\tilde{J}_{1234}$, we perform a numerical calculation with the thicknesses $d_1 = d_2 = d_3 = 1$ nm for all three nonmagnetic layers, and the thicknesses $L_2 = L_3 = 2$ nm for the two ferromagnetic layers F_2 and F_3. All other material parameters are the same as before. Figure 5 shows the calculation results, and from the amplitudes we find the NN IEC strength $\tilde{J}_{34} = 5.34$ mJ/m^2, the NNN IEC strength $\tilde{J}_{234} = 1.61$ mJ/m^2, and the NNNN IEC strength $\tilde{J}_{1234} = -0.15$ mJ/m^2. Thus the strength of the IEC becomes progressively smaller for longer-range coupling. The values of NN and NNN IEC constants $\tilde{J}_{34}$ and $\tilde{J}_{234}$ are similar but slightly different from the corresponding constants $\tilde{J}_{23}$ and $\tilde{J}_{123}$ in the FNFNF system (Fig. 2). Interestingly, the differences are of the same order as $\tilde{J}_{1234}$. The differences can be understood

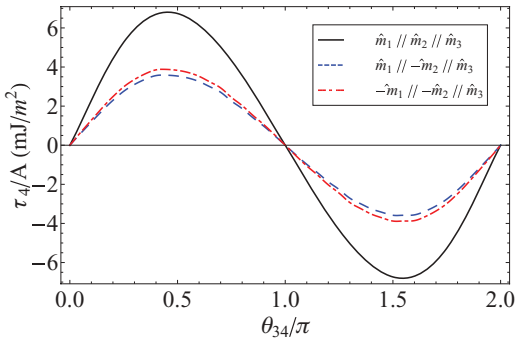

FIG. 5. (Color online) The torque τ_4 acting on the magnetization of F_4 as a function of θ_{34}. The deviation between red (dotted-dashed) and blue (dotted) lines shows the existence of the interaction between F_1 and F_4.

as follows: If $\hat{\mathbf{m}}_1//\hat{\mathbf{m}}_2$ and the spin information loss in N_1 is negligible, the leftmost FNF layers in the FNFNFNF system may be regarded as a single F layer and the FNFNFNF system reduces to the FNFNF system. In this reduction, the *sum* of the NNN IEC and the NNNN IEC in the FNFNFNF system should be identified with the NNN IEC in the FNFNF system, which explains why the difference between $\tilde{J}_{234}$ in the FNFNFNF system and $\tilde{J}_{123}$ in the FNFNF system is of the order of $\tilde{J}_{1234}$. In turn, this difference in the NNN IEC constants can propagate to the evaluation of the NN IEC constants, as supported by the excellent agreement between $\tilde{J}_{34} + \tilde{J}_{234}$ for the FNFNFNF system and $\tilde{J}_{23} + \tilde{J}_{123}$ for the FNFNF system (a difference of only 0.04 mJ/m^2). Thus the differences of the IEC constants in the FNFNFNF and FNFNF systems are natural consequences of the long-range nature of the IEC.

In summary, we have calculated the IEC energy via a spin-transfer torque in a free-electron model. The (perpendicular) spin-transfer torque, which is an angle derivative of the energy and has sine dependence, depends on magnetic configurations. From these results, we can deduce that the energy has an angle dependence of the form of Eq. (10), indicating the existence of the NNN IEC. The strength of the NNN IEC is generally smaller than the NN IEC. Nevertheless, our estimation indicates that the strength of the NNN IEC is large enough to allow for its experimental detection.

ACKNOWLEDGMENTS

We acknowledge Shanghoon Lee, J.-H. Chung, and Kyung-Jin Lee at Korea University for valuable discussions and providing motivations for this problem. This work was funded by the NRF (2010-0014109, 2010-0023798) and BK21.

APPENDIX A: IEC IN LARGE LAYER THICKNESS LIMIT

In this Appendix, we will calculate NN IEC and NNN IEC in a large layer thickness limit using Bruno's free-electron model.[18,23] To do so, we regard $F_1N_1F_2$ in the $F_1N_1F_2N_2F_3$ system as a single synthetic ferromagnetic layer, say F_A, and apply Bruno's formula to evaluate the IEC in F_ANF_B ($F_B = F_3$, $N = N_2$). Bruno's formula reads as follows [Eqs. (1) and (4)

in Ref. 23],

$$J_1 = -\frac{1}{4\pi^3}\mathrm{Im}\int d^2\vec{k}_\parallel \int_{-\infty}^{\infty} d\varepsilon f(\varepsilon) \times \frac{2\Delta r_A \Delta r_B e^{iq_z D}}{1-2\bar{r}_A\bar{r}_B e^{iq_z D}+\left(\bar{r}_A^2-\Delta r_A^2\right)\left(\bar{r}_B^2-\Delta r_B^2\right)e^{iq_z D}} \tag{A1}$$

where q_z is change in the electron wave vector impinging from N to F and reflecting back, D is the thickness of the N layer ($D = d_2$ in our system), $f(\varepsilon)$ is the Fermi-Dirac function, $\bar{r}_{A,B} = (r^{\uparrow}_{A,B} + r^{\downarrow}_{A,B})/2$, $\Delta r_{A,B} = (r^{\uparrow}_{A,B} - r^{\downarrow}_{A,B})/2$, and $r^{\uparrow,\downarrow}_{A,B}$ is the reflection coefficient of up and down electrons reflecting F_A and F_B with obvious notation.

Here, we generalize Ref. 23 a little more, and the majority spin electrons are not assumed to be reflectionless. In our case, $r_A^{\uparrow,\downarrow}$ have a dependence on the angle between the magnetizations of F_1 and F_2. We can calculate $r_A^{\uparrow,\downarrow}$ as a function of $\cos\theta_{12}$ and expand it into a Taylor series in powers of $\cos\theta_{12}$ up to first order. These r's are also functions of $r_\infty^{\uparrow}$ and $r_\infty^{\downarrow}$, which are reflection coefficients of electrons incident from the nonmagnetic layer to a semi-infinite ferromagnetic layer having a majority and minority spin, respectively.

Inserting the results for r's into Eq. (A2), we have J_1 in the form of $J_1 = \tilde{J}_{23} + \tilde{J}_{123}\cos\theta_{12}$. In the large layer thickness limit, we can obtain a simple expression for $\tilde{J}_{23}$ and $\tilde{J}_{123}$, since there are many cancellations during the integration: Oscillatory components with different wave vectors cancel each other except for the Fermi wave vector k_F, which is a stationary value in $\vec{k}_\parallel$ (critical spanning vector).[17,18,23] Then we have

$$\begin{aligned}\tilde{J}_{23} = \frac{1}{4\pi^2}\frac{\hbar^2}{2m}\mathrm{Im}\Bigg(e^{2ik_F d_2}\Bigg\{&\frac{1}{2}(r_\infty^{\uparrow}-r_\infty^{\downarrow})^2\left(\frac{d_2}{k_F}\right)^{-2} \\ &+e^{2ik_F^{\uparrow}L}\left[-\frac{1}{2}(r_\infty^{\uparrow}-r_\infty^{\downarrow})r_\infty^{\uparrow}(1-r_\infty^{\uparrow 2})\left(\frac{d_2}{k_F}+\frac{L_1}{k_F^{\uparrow}}\right)^{-2}+\frac{1}{4}(r_\infty^{\uparrow 2}-r_\infty^{\downarrow 2})(1-r_\infty^{\uparrow 2})^2\left(\frac{d_2}{k_F}+\frac{L}{k_F^{\uparrow}}+\frac{d_1}{k_F}\right)^{-2}e^{2ik_F d_1}\right] \\ &+e^{2ik_F^{\downarrow}L}\left[\frac{1}{2}(r_\infty^{\uparrow}-r_\infty^{\downarrow})r_\infty^{\downarrow}(1-r_\infty^{\downarrow 2})\left(\frac{d_2}{k_F}+\frac{L_1}{k_F^{\downarrow}}\right)^{-2}-\frac{1}{4}(r_\infty^{\uparrow 2}-r_\infty^{\downarrow 2})(1-r_\infty^{\downarrow 2})^2\left(\frac{d_2}{k_F}+\frac{L}{k_F^{\downarrow}}+\frac{d_1}{k_F}\right)^{-2}e^{2ik_F d_1}\right]\Bigg\}\Bigg)\end{aligned} \tag{A2}$$

$$\begin{aligned}\tilde{J}_{123} = \frac{1}{4\pi^2}\frac{\hbar^2}{2m}\mathrm{Im}\Bigg[&\frac{1}{4}(r_\infty^{\uparrow 2}-r_\infty^{\downarrow 2})(1-r_\infty^{\uparrow 2})^2\left(\frac{d_2}{k_F}+\frac{L}{k_F^{\uparrow}}+\frac{d_1}{k_F}\right)^{-2}e^{2ik_F d_1+2ik_F^{\uparrow}L+2ik_F d_2} \\ &+\frac{1}{4}(r_\infty^{\uparrow 2}-r_\infty^{\downarrow 2})(1-r_\infty^{\downarrow 2})^2\left(\frac{d_2}{k_F}+\frac{L}{k_F^{\downarrow}}+\frac{d_1}{k_F}\right)^{-2}e^{2ik_F d_1+2ik_F^{\downarrow}L+2ik_F d_2}\Bigg],\end{aligned} \tag{A3}$$

which have the same form as Eqs. (11) and (12), respectively.

APPENDIX B :SMALL F_2 THICKNESS

For very small L, the spin component perpendicular to $\hat{\mathbf{m}}_2$ may not completely decay in F_2, thereby opening an additional channel for the NNN coupling. In this situation, the third term in Eq. (10) cannot fully capture the NNN coupling. To explore this possibility, we calculate τ_3/A in terms of θ_{23} for a small thickness of F_2, $L = 0.5$ nm. Other parameters are the same as those in the main text. We can see that for a perpendicular configuration ($\hat{\mathbf{m}}_1 \perp \hat{\mathbf{m}}_2$) the angle dependences are shifted with respect to the corresponding dependence for the parallel ($\hat{\mathbf{m}}_1 // \hat{\mathbf{m}}_2$) or antiparallel ($\hat{\mathbf{m}}_1 // -\hat{\mathbf{m}}_2$) configurations (Fig. 6). This shift indicates that for a conduction electron originating from F_1, its transverse spin component perpendicular to $\hat{\mathbf{m}}_2$ still survives even after passing through F_2. In the limit $L \to 0$, the transverse component is as likely to survive as the longitudinal component after passing through F_2, and in this limiting case, the NNN IEC should be the Heisenberg-like form proportional to $(\hat{\mathbf{m}}_1 \cdot \hat{\mathbf{m}}_3)$. If this limiting case were achieved, the result for the perpendicular configuration ($\hat{\mathbf{m}}_1 \perp \hat{\mathbf{m}}_2$) in Fig. 6 should have exhibited the relative phase shift of $\pi/2$. However, the actual phase shift is only about one third of the expected value, which indicates that even for $L = 0.5$ nm the longitudinal component still survives significantly better than the transverse component after passing through F_2. As increasing the thickness of F_2, the shift of the sinusoidal functions becomes smaller and essentially disappears for $L \geqslant 1$ nm, justifying the analysis in the main text. For our parameter set, this threshold value of L is comparable to $l_{\mathrm{dep}} \equiv 2\pi/(k^{\uparrow}_{F_2} - k^{\downarrow}_{F_2}) = 0.9$ nm.

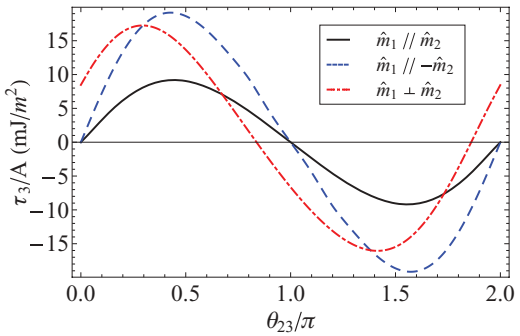

FIG. 6. (Color online) The torque τ_3 acting on the magnetization of F_3 as a function of θ_{23} with $L = 0.5$ nm, which is smaller than l_{dep}.

[1]M. N. Baibich, J. M. Broto, A. Fert, F. Nguyen Van Dau, F. Petroff, P. Etienne, G. Creuzet, A. Friederich, and J. Chazelas, Phys. Rev. Lett. **61**, 2472 (1988).
[2]G. Binasch, P. Grünberg, F. Saurenbach, and W. Zinn, Phys. Rev. B **39**, 4828 (1989).
[3]S. S. P. Parkin, N. More, and K. P. Roche, Phys. Rev. Lett. **64**, 2304 (1990).
[4]S. S. P. Parkin, Phys. Rev. Lett. **67**, 3598 (1991).
[5]F. Petroff, A. Barthélemy, D. H. Mosca, D. K. Lottis, A. Fert, P. A. Schroeder, W. P. Pratt, Jr., R. Loloee, and S. Lequien, Phys. Rev. B **44**, 5355 (1991).
[6]K. Ounadjela, D. Muller, A. Dinia, A. Arbaoui, P. Panissod, and G. Suran, Phys. Rev. B **45**, 7768 (1992).
[7]J. Fassbender, F. Nörtemann, R. L. Stamps, R. E. Camley, B. Hillebrands, G. Güntherodt, and S. S. P. Parkin, Phys. Rev. B **46**, 5810 (1992).
[8]Y. Huai and R. W. Cochrane, J. Appl. Phys. **72**, 2523 (1992).
[9]Z. Q. Qiu, J. Pearson, and S. D. Bader, Phys. Rev. B **46**, 8659 (1992).
[10]M. T. Johnson, S. T. Purcell, N. W. E. McGee, R. Coehoorn, J. aan de Stegge, and W. Hoving, Phys. Rev. Lett. **68**, 2688 (1992).
[11]P. J. H. Bloemen, R. van Dalen, W. J. M. de Jonge, M. T. Johnson, and J. aan de Stegge, J. Appl. Phys. **73**, 5972 (1993).
[12]J. Unguris, R. J. Celotta, and D. T. Pierce, Phys. Rev. Lett. **67**, 140 (1991).
[13]S. Demokritov, J. A. Wolf, and P. Grünberg, Europhys. Lett. **15**, 881 (1991).
[14]S. T. Purcell, W. Folkerts, M. T. Johnson, N. W. E. McGee, K. Jager, J. aan de Stegge, W. B. Zeper, W. Hoving, and P. Grünberg, Phys. Rev. Lett. **67**, 903 (1991).
[15]Z. Celinski and B. Heinrich, J. Magn. Magn. Mater. **99**, L25 (1991).
[16]A. Fuß, S. Demokritov, P. Grünberg, and W. Zinn, J. Magn. Magn. Mater. **103**, L221 (1992).
[17]P. Bruno and C. Chappert, Phys. Rev. Lett. **67**, 1602 (1991).
[18]P. Bruno, J. Magn. Magn. Mater. **121**, 238 (1993).
[19]M. D. Stiles, Phys. Rev. B **48**, 7238 (1993).
[20]P. Bruno, Phys. Rev. B **52**, 411 (1995).
[21]P. J. H. Bloemen, M. T. Johnson, M. T. H. van de Vorst, R. Coehoorn, A. Reinders, J. aan de Stegge, R. Jungblut, and W. J. M. de Jonge, J. Magn. Magn. Mater. **148**, 193 (1995).
[22]J. J. de Vries, A. A. P. Schudelaro, R. Jungblut, P. J. H. Bloemen, A. Reinders, J. Kohlhepp, R. Coehoorn, and W. J. M. de Jonge, Phys. Rev. Lett. **75**, 4306 (1995).
[23]P. Bruno, Europhys. Lett. **23**, 615 (1993).
[24]J. C. Slonczewski, J. Magn. Magn. Mater. **159**, L1 (1996).
[25]L. Berger, Phys. Rev. B **54**, 9353 (1996).
[26]Z. Li and S. Zhang, Phys. Rev. B **68**, 024404 (2003).
[27]G. A. Prinz, Science **282**, 5394 (1998).
[28]E. B. Myers, D. C. Ralph1, J. A. Katine, R. N. Louie, and R. A. Buhrman, Science **285**, 867 (1999).
[29]S. I. Kiselev, J. C. Sankey, I. N. Krivorotov, N. C. Emley, R. J. Schoelkopf, R. A. Buhrman, and D. C. Ralph, Nature (London) **425**, 380 (2003).
[30]D. Houssameddine, U. Ebels, B. Delaët, B. Rodmacq, I. Firastrau, F. Ponthenier, M. Brunet, C. Thirion, J.-P. Michel, L. Prejbeanu-Buda, M.-C. Cyrille, O. Redon, and B. Dieny, Nat. Mater. **6**, 447 (2007).
[31]H. A. M. van den Berg, W. Clemens, G. Gieres, G. Rupp, W. Schelter, and M. Vieth, IEEE Trans. Magn. **32**, 4624 (1996).
[32]J. L. Leal and M. H. Kryder, J. Appl. Phys. **83**, 3720 (1998).
[33]J. C. Slonczewski, Phys. Rev. B **39**, 6995 (1989).
[34]M. D. Stiles and A. Zangwill, Phys. Rev. B **66**, 014407 (2002).
[35]J. C. Sankey, Y.-T. Cui, J. Z. Sun, J. C. Slonczewski, R. A. Buhrman, and D. C. Ralph, Nat. Phys. **4**, 67 (2008).
[36]H. Kubota, A. Fukushima, K. Yakushiji, T. Nagahama, S. Yuasa, K. Ando, H. Maehara, Y. Nagamine, K. Tsunekawa, D. D. Djayaprawira, N. Watanabe, and Y. Suzuki, Nat. Phys. **4**, 37 (2008).
[37]S.-C. Oh, S.-Y. Park, A. Manchon, M. Chshiev, J.-H. Han, H.-W. Lee, J.-E. Lee, K.-T. Nam, Y. Jo, Y.-C. Kong, B. Dieny, and K.-J. Lee, Nat. Phys. **5**, 898 (2009).
[38]C. Wang, Y.-T. Cui, J. A. Katine, R. A. Buhrman, and D. C. Ralph, Nat. Phys. **7**, 496 (2011).
[39]S.-Y. Park, Y. Jo, and K.-J. Lee, Phys. Rev. B **84**, 214417 (2011).
[40]I. Theodonis, N. Kioussis, A. Kalitsov, M. Chshiev, and W. H. Butler, Phys. Rev. Lett. **97**, 237205 (2006).
[41]C. Heiliger and M. D. Stiles, Phys. Rev. Lett. **100**, 186805 (2008).
[42]C.-Y. You, J. Magn. **17**, 73 (2012)
[43]M. Wilczyński, J. Barnaś, and R. Świrkowicz, Phys. Rev. B **77**, 054434 (2008).